Soft Matter

PAPER

View Article Online
View Journal | View Issue

Cite this: *Soft Matter*, 2014, **10**, 3200

Effects of molecular geometry on the self-assembly of giant polymer–dendron conjugates in condensed state†

Xue-Hui Dong,[a] Xiaocun Lu,[a] Bo Ni,[a] Ziran Chen,[a] Kan Yue,[a] Yiwen Li,[a] Lixia Rong,[b] Tadanori Koga,[c] Benjamin S. Hsiao,[b] George R. Newkome,[a] An-Chang Shi,*[d] Wen-Bin Zhang*[ae] and Stephen Z. D. Cheng*[a]

Received 1st August 2013
Accepted 26th February 2014

DOI: 10.1039/c3sm52087k

www.rsc.org/softmatter

A series of giant polymer–dendron conjugates with a dendron head and a linear polymer tail were synthesized *via* "click" chemistry between azide-functionalized polystyrene (PS_N, *N*: degree-of-polymerization) and *t*-butyl protected, alkyne-functionalized second generation dendron (*t*D), followed by a deprotection process to generate a dendron termini possessing nine carboxylic acid groups. The molecular structures were confirmed by nuclear magnetic resonance, size-exclusion chromatographic analyses, and matrix-assisted laser desorption ionization time-of-flight mass spectra. These well-defined conjugates can serve as a model system to study the effects of the molecular geometries on the self-assembly behaviour, as compared with their linear analogues. Four phase morphologies found in flexible linear diblock copolymer systems, including lamellae, bicontinuous double gyroids, hexagonal packed cylinders, and body-centred cubic packed spheres, were observed in this series of conjugates based on the results of small angle X-ray scattering and transmission electron microscopy. All of the domain sizes in these phase separated structures were around or less than 10 nm. A 'half' phase diagram was constructed based on the experimental results. The geometrical effect was found not only to enhance the immiscibility between the PS_N tail and dendron head, but also systematically shift all of the phase boundaries towards higher volume fractions of the PS_N tails, resulting in an asymmetrical phase diagram. This study may provide a pathway to the construction of ordered patterns of sub-10 nm feature size using polymer–dendron conjugates.

Introduction

Block copolymers with chemically distinct components have continued to attract attention for their capability to form periodic structures at nanometer scale.[1,2] The structural formation of diblock copolymers depends mainly on three experimentally accessible parameters based on the mean-field theory: the overall degree-of-polymerization *N*, the Flory–Huggins interaction parameter χ, and the volume fractions of the copolymer components *f*.[2] By carefully tuning these parameters, four thermodynamically stable phases, including lamellae (Lam), bicontinuous double gyroids (DG), hexagonal packed cylinders (Hex), and body-centred cubic packed spheres (BCC), together with several metastable phases, have been theoretically predicted[3–7] and experimentally observed.[2,8–15] While linear block copolymers have been extensively studied for decades, they continue to fascinate the scientific community but the focus has shifted to the polymers with versatile architectures, such as star polymers,[16–18] cyclic polymers,[19–23] hyperbranched polymers,[24–26] *etc.*, encouraged by the development of more sophisticated synthetic techniques.[27,28] Incorporation of architectural factors expands the scope and utility of block copolymers and instills novel self-assembly behaviours.[26]

One of the most promising applications of block copolymers is, *via* integrating the top-down lithographic approach, to construct nanoscale ordered structures as templates,[29,30] in particular, for the periodic patterns with sub-20 nm feature size.[31–33] To generate periodic patterns at such a length scale, it requires that the overall degree-of-polymerization (*N*) must be sufficient small since the dimension of the patterns is proportional to $N^{2/3}$ at the strong-segregation region.[33] Unfortunately, due to weak interactions between the majority of conventional

[a]*Department of Polymer Science, College of Polymer Science and Polymer Engineering, The University of Akron, Akron, OH 44325-3909, USA. E-mail: scheng@uakron.edu; wz8@uakron.edu; Fax: +1 330 972 8626; Tel: +1 330 972 6931; +1 330 990 9801*

[b]*Department of Chemistry, Stony Brook University, Stony Brook, New York, 11794-3400, USA*

[c]*Chemical and Molecular Engineering Program, Stony Brook University, Stony Brook, New York, 11794-2275, USA*

[d]*Department of Physics and Astronomy, McMaster University, Hamilton, Ontario L8S 4M1, Canada. E-mail: shi@mcmaster.ca; Fax: +1 905 521 2773; Tel: +1 905 525 140*

[e]*Key Laboratory of Polymer Chemistry and Physics of Ministry of Education, College of Chemistry and Molecular Engineering, Center for Soft Matter Science and Engineering, Peking University, Beijing 100871, China*

† Electronic supplementary information (ESI) available: The syntheses and detailed experimental procedures were described. See DOI: 10.1039/c3sm52087k

blocks in copolymers, the N value has to be large enough in order to achieve their phase separations and obtain structures which are long-range ordered ($\chi N \geq 10$).[1,2] Ion complexation with block copolymer was found to affect the effective χ interaction parameter.[34–38] On the other hand, design and synthesis of new block components with higher χ values represent a more general approach to achieve even smaller spacing motifs. For example, Willson *et al.* reported a novel block copolymer, poly(trimethylsilylstyrene)-*block*-polylactide with a χ value of around 0.4, capable of forming an ordered pattern as small as ~5 nm.[31] Later, other specifically designed poly(trimethylsilylstyrene)-containing block polymers with high repulsion interactions, have been demonstrated to form sub-10 nm lamellae with a perpendicular orientation at a given substrate using a top coat necessary to neutralized the top interface.[39]

On the other hand, theoretical predictions show that the phase behaviours of block copolymers with complicated architectures can be different from their linear analogues.[40–45] Among them, great interests have been paid to the cyclic, hyperbranched, and dendritic polymers.[18,22,26] Experimentally, Hawker and co-workers reported a ~30% decrease in the domain spacing with cyclic polystyrene-*block*-poly(ethylene oxide) (PS-*b*-PEO), when compared with their corresponding linear analogues.[22] The geometrical differences from the linear flexible diblock copolymers may lead not only to a change of phase boundaries of the ordered structures, but also to the order–disorder transition temperatures as insightfully explained by theoretic predictions.[41,42] It is thus possible to achieve phase separations at reduced feature sizes with block polymers based on conventional monomers by replacing one of the linear blocks with different structural architectures.

Dendritic molecules provide an excellent prototype to study the molecular geometrical effects on the self-assembly behaviours, due to their precisely defined chemical structures, tailorable size, and versatile functionalities.[46] Though dendrimers have been extensively studied in the areas of drug delivery, metal nanoparticle preparation, catalyst, and other useful techniques,[47,48] the self-assembly behaviour of polymer–dendron giant conjugates are not yet fully understood, especially in condensed state.[26] The simplest giant conjugate is a dendron head tethered with a linear polymer tail. Meijer's group first reported the bulk self-assembly of polymer–dendron giant conjugates consisting of a linear PS tail and a carboxylic acid-functionalized poly(propylene imine) dendritic termini.[49] Ordered structures were observed *via* small angle X-ray scattering (SAXS) and transmission electron microscopy (TEM) experiments. With increasing the generation, *i.e.* the number of carboxylic acid groups and the volume fraction of the dendrimers, a Hex to Lam transition in the phase-separated structures was observed.[49] Mackay *et al.* later studied another system without a strong phase separation driving force, constructed by a poly(benzyl ether) dendron and a linear PS tail.[50] An entropic factor resulted from the impenetrability of dendron by the linear tails was invoked to explain the formation of ordered structures. The clear impact of molecular architectures on the phase separated structures at given volume fractions can be identified by comparing with the conformationally symmetric, linear flexible diblock copolymers.[49–52] In both reports, only Lam and Hex phases were observed. Other structures found in those linear diblock copolymers,[2] *e.g.*, DG and BCC structures, were not reported, due possibly to either the difficulties in facile synthesis of their samples to cover entire volume fractions, or specific molecular geometric effects necessary to alter the phase stabilities.

In this article, we report the synthesis of a series of giant PS–dendron (PS_N–D) conjugates. The self-assembly in condensed state has been studied *via* SAXS and TEM. Four phase-separated structures, Lam, DG, Hex, and BCC phases are identified. More importantly, it is found that phase separation is achieved in a low N range that is forbidden in their linear flexible analogues, such as in PS-*block*-poly(acrylic acid) (PS-*b*-PAA). The resulting ordered structures possess a domain size around or less than 10 nm. Furthermore, the experimentally observed phase boundaries are asymmetrically shifted to larger volume fractions of PS (f_{PS}) when compared to their linear analogue. The dendritic geometry thus affects the phase boundaries *via* the change of the phase separation ability (the vertical axis in the phase diagram, represented as the reciprocal temperature) and the volume fraction (the horizontal axis in the phase diagram) at which phase transition occurs.

Experimental section

Chemicals and solvents

The following chemicals are used, as received: sodium azide (NaN_3, Aldrich, ReagentPlus®, > 99.5%), *N*,*N*-dimethylformamide (DMF, Aldrich, 99.9%), methanol (MeOH, Fisher Scientific, reagent grade), hydroxybenzotriazole (HOBT, Aldrich, 97%), *N*,*N*′-diisopropylcarbodiimide (DIPC, Aldrich, 99%), trifluoroacetic acid (TFA, ReagentPlus®, 99%), deuterated chloroform ($CDCl_3$, Aldrich, 99.8 atom% D), *N*,*N*,*N*′,*N*″,*N*″-pentamethyldiethylenetriamine (PMDETA, Aldrich, 99%). cuprous bromide (CuBr, Aldrich, 98%) was purified by stirring in $MeCO_2H$ overnight, washed with acetone for three times, and dried *in vacuo*. Chloroform ($CHCl_3$, Fisher Scientific, reagent grade) and styrene (Aldrich, 99%) were purified by stirring over CaH_2 for 12 hours and redistilled *in vacuo* before use. The second generation Newkome-type dendron (*t*-butyl protected) was prepared according to reported procedures.[53] Preparation of the polystyrene *via* ATRP (PS–Br) and azide-functionalized polystyrene ($PS–N_3$) are described in literatures.[54]

Instrumentation and characterizations

All ^1H and ^{13}C NMR spectra were acquired in $CDCl_3$ using a Varian 500 NMR spectrometer. The ^1H NMR spectra were referenced to the residual proton impurities in the $CDCl_3$ at δ 7.27 ppm. The ^{13}C NMR spectra were referenced to $^{13}CDCl_3$ at δ 77.00 ppm.

Infrared spectra were recorded on an Excalibur Series FT-IR spectrometer (DIGILAB, Randolph, MA) by casting polymer films onto KBr plates from polymer solutions. The data were processed using Win-IR software.

Size-exclusion chromatographic analyses (SEC) were performed using a Waters 150-C Plus instrument equipped with

three HR-Styragel columns [100 Å, mixed bed (50/500/10^3/10^4 Å), mixed bed (10^3/10^4/10^6 Å)] and a double detector system with THF, as eluent, at a flow rate of 1.0 mL min^{-1} at 30 °C; the detector system consisted of a differential refractometer (Waters 410) and a laser light scattering detector (Wyatt Technology, DAWN EOS, λ = 670 nm). Regular SEC calibrations were conducted with polystyrene standards (Polymer Laboratories).

Matrix-assisted laser desorption ionization time-of-flight (MALDI-TOF) mass spectra were recorded on a Bruker Reflex-III TOF mass spectrometer (Bruker Daltonics, Billerica, MA). The instrument was equipped with an LSI model VSL-337ND pulsed 337 nm nitrogen laser (3 nm pulse width), a single-stage pulsed ion extraction source, and a two-stage gridless reflector. *trans*-2-[3-(4-*tert*-Butylphenyl)-2-methyl-2-propenylidene]-malononitrile (DCTB, Aldrich, > 98%) served as matrix and silver trifluoroacetate as cationizing agent.

Small angle X-ray scattering (SAXS) experiments were conducted on the beamline X27C at the National Synchrotron Light Source (NSLS), Brookhaven National Laboratory (BNL). The wavelength of X-ray is 0.1371 nm. The collection time for each sample was 10 to 60 s, depending on the scattering intensity. Two-dimensional SAXS patterns were acquired using a MAR-CCD detector. The scattering pattern was calibrated with silver behenate standards with the primary reflection peak (1.067 nm^{-1}). Data were processed with the software Polar (Stony Brook Technology and Applied Research, Stony Brook, New York).

Transmission electron microscopy (TEM, JEOL 1200 EXII) was measured with an accelerating voltage of 120 kV. Thin slices of samples were prepared by microtoming using a Reichert Ultracut S (Leica) ultra-cryomicrotome machine at room temperature. The samples were stained with RuO_4 vapour at room temperature for 20 minutes to increase contrast.

Density of alkyne-functionalized dendron with nine carboxylic acid groups (alkyne–D) was measured using a mixture solvent of CCl_4 and hexanes. The sample was heated on a hot stage to 90 °C for 1 h under nitrogen protection to eliminate any bubbles. A small piece of solid sample was added into the CCl_4. Slow adding hexanes until the sample was suspended in the mixtures and stabilized for 2 days. The density at 25, 50, and 75 °C was measured to be 1.233, 1.226, and 1.219 g cm^{-3}, respectively. Density of polystyrene is 1.052 g cm^{-3} at room temperature according to literature.[55] The volume fraction of PS (f_{PS}) was calculated based on the following equation,

$$f_{PS} = \frac{M_n^{PS}/\rho_{PS}}{M_n^{PS}/\rho_{PS} + M^D/\rho_D} \quad (1)$$

where M_n^{PS} and M^D are the molecular weight of PS chain and carboxylic acid functionalized dendron, respectively.

General synthetic procedures

Synthesis of alkyne functionalized, *t*-butyl protected G2 dendron (alkyne–*t*D). The second generation Newkome-type dendron (220 mg, 153 μmol), 4-pentynoic acid (18 mg, 183 μmol), and HOBT (24.7 mg, 183 μmol) was dissolved anhydrous CH_2Cl_2 (10 mL). After cooling to 0 °C in an ice bath, DIPC (23 mg, 183 μmol) was added dropwise with stirring. The mixture was brought to room temperature and stirred for 24 h. The alkyne functionalized, *t*-butyl protected G2 dendron (alkyne–*t*D) was eluted with a mixture of EtOAc: hexanes (1 : 5 v/v) (195 mg, 82% yield). ^{1}H NMR ($CDCl_3$, 500 MHz, ppm, δ): 6.05 (s, 4H, –CH_2(C=O)N*H*–), 2.51 (t, 2H, –C*H*$_2$$CH_2$–), 2.33 (t, 2H, –$CH_2$C*H*$_2$–), 2.21 (t, 24H, –$CH_2$C*H*$_2$(C=O)NH–), 1.94 (t, 24H, –C*H*$_2$$CH_2$(C=O)NH–), 2.03 (t, 1H, C*H*CCH_2–), 1.43 (s, 81H, –OC(CH_3)$_3$). ^{13}C NMR ($CDCl_3$, 500 MHz, ppm, δ): 173.1, 171.3, 83.7, 80.7, 69.4, 58.0, 57.6, 36.1, 32.4, 32.0, 30.0, 28.2, 15.1. MS (MALDI-TOF): calcd: 1541.97, found: 1542.18 $(M\cdot Na)^+$.

Typical procedure for the preparation of *t*-butyl protected giant conjugates PS_N–*t*D. PS_N–N_3 (200 mg, 2000 g mol^{-1}, 100 μmol), alkyne–*t*D (137 mg, 90 μmol), CuBr (12 mg, 100 μmol), and anhydrous toluene (15 mL) were added into an Schlenk flask. After three freeze–pump–thaw cycles, PMDETA (17 mg, 100 μmol) was introduced into the flask under nitrogen. After stirring overnight under 20 °C, the solution was applied onto a short silica gel column to remove the CuBr salt. Excess PS was removed by elution with toluene. Further eluting with a mixture of $CHCl_3$ and MeOH (95 : 5 v/v) gave the product, which was concentrated and precipitated in the cold methanol (287 mg, 91%). ^{1}H NMR ($CDCl_3$, 500 MHz, ppm, δ): 6.30–7.40 (br, 95H, phenyl rings), 6.13 (s, 4H, –CH_2(C=O)N*H*–), 4.90–5.20 (m, 1H, –CH_2C*H*(–Ar)–triazole–), 3.40–3.75 (m, 2H, CH_3C*H*$_2$O(C=O)–), 2.91 (m, 2H, –triazole–C*H*$_2$$CH_2$–), 2.38 (m, 2H, –triazole–CH_2C*H*$_2$–), 2.18 (t, 24H, –CH_2C*H*$_2$(C=O)NH–), 1.94 (t, 24H, –C*H*$_2$$CH_2$(C=O)NH–), 1.67–2.15 (br, 19H, –CH_2C*H*(–Ar)–), 1.20–1.67 [br, 38H, –C*H*$_2$CH(–Ar)–], 1.43 [s, 81H, –OC(C*H*$_3$)$_3$], 0.93 [m, 6H, –O(C=O)C(C*H*$_3$)$_2$$CH_2$–]; ^{13}C NMR ($CDCl_3$, 500 MHz, ppm, δ): 172.6, 144.8, 128.6, 125.4, 80.6, 59.6, 57.2, 43.9, 40.2, 31.4, 29.8, 28.1, 13.9; FT-IR (cm^{-1}): 3082, 3060, 3027, 2926, 2852, 2098, 1944, 1884, 1807, 1730, 1601, 1491, 1450, 1367, 1314, 1153, 1069, 1029, 908, 848, 756, 698, 540; SEC (THF, RI detector): M_n = 3800 g mol^{-1}, M_w = 3900 g mol^{-1}, $Đ_M$ = 1.03. MS (MALDI-TOF): calcd: 3363.83, found: 3363.96 $(M\cdot Na)^+$.

Typical procedure for preparation of giant conjugates PS_N–D. PS_N–*t*D (200 mg, 57 μmol), TFA (200 mg, 1.75 mmol), and anhydrous $CHCl_3$ (10 mL) were added into a round bottom flask equipped with a magnetic stirrer. The solution was stirred overnight under nitrogen protection at 20 °C. Solvent, excess TFA, and by-products were removed by rotatory evaporation. The product was further dried in the vacuum oven overnight (163 mg, 95%). ^{1}H NMR ($CDCl_3$, 500 MHz, ppm, δ): 6.30–7.40 (br, 95H, phenyl rings), 4.90–5.20 (m, 1H, –CH_2C*H*–(–Ar)–triazole–), 3.40–3.75 [m, 2H, MeC*H*$_2$O(C=O)–], 2.15–3.0 (br), 1.67–2.15 [br, 19H, –CH_2C*H*(–Ar)–], 1.20–1.67 [br, 38H, –C*H*$_2$CH(–Ar)–], 0.93 [m, 6H, –O(C=O)C(C*H*$_3$)$_2$$CH_2$–]; ^{13}C NMR ($CDCl_3$, 500 MHz, ppm, δ): 145.2, 127.9, 125.6, 59.9, 43.9, 40.4, 13.9; FT-IR (cm^{-1}): 3082, 3060, 3027, 2926, 2852, 1944, 1884, 1807, 1723, 1660, 1601, 1548, 1493, 1450, 1197, 1153, 1067, 1029, 908, 758, 698, 541; SEC (THF, RI detector): M_n = 3400 g mol^{-1}, M_w = 3600 g mol^{-1}, $Đ_M$ = 1.03; MS (MALDI-TOF): calcd: 2859.32, found: 2860.26 $(M\cdot Na)^+$; calc.: 2875.41, found: 2876.24 $(M\cdot K)^+$.

Results and discussions

Preparation of the giant polymer–dendron conjugates

The synthetic route to the giant polymer–dendron conjugates is illustrated in Scheme 1. Polystyrene tails with different N values were prepared *via* atom-transfer radical polymerization (ATRP) according to previous reports.[54,56] Ethyl-2-bromoisobutyrate was used as the initiator and the N value was controlled by the polymerization time. To construct the phase diagram, PS_N tails with $N = 16$ to 150 were synthesized. The products were fully characterized by SEC and NMR (Fig. S1 and S2 in ESI†). All SEC traces of the PS homopolymers are symmetric, with polydispersity index ($Đ_M$) less than 1.10. The shift of elution volume is in good agreement as the N value increases (Fig. S1 in ESI† and Table 1). A typical ^{1}H NMR spectrum is shown in Fig. S2 in ESI,† in which chemical shifts of styrene repeat unit are identified. The molecular characterizations are summarized in Table 1.

The terminal bromide group at one of the PS_N chain ends can be readily converted into azide group,[54,56] and the conversion can be monitored *via* FT-IR spectroscopy. A unique absorption for the azide group is observed at ~2100 cm^{-1} (Fig. S3 in ESI†). This substitution is also confirmed by ^{1}H NMR. The terminal proton, adjunct to the bromide group, shifts from 4.51 to 4.05 ppm (Fig. 1a and S2†).[54] These azide terminated PS_N chains were then coupled with the alkyne–*t*D using "click" chemistry in high yield, as shown in Scheme 1. The absorption band at 2100 cm^{-1} completely disappeared after the conversion to the triazole, confirming that the azide group has been fully consumed (Fig. S3 in ESI†). The intensity of an absorption band at ~1729 cm^{-1}, corresponding to the C=O groups, increases due to the dendron incorporation (Fig. S3 in ESI†). ^{1}H NMR spectrum provides clear identifications of the structure, as shown in Fig. 1b. The chemical shifts from the *t*D can be clearly observed at 6.16 (d), 2.88 (b), 2.36 (c), 2.12 (f), 1.90 (j), and 1.41 ppm (l) (j and l are not labeled due to their high intensities). The shift of proton k from 4.00 to 5.00 ppm is due to the formation of the triazole ring. The SEC traces (Fig. 2, red) show a shift toward lower retention volumes, indicating hydrodynamic volume

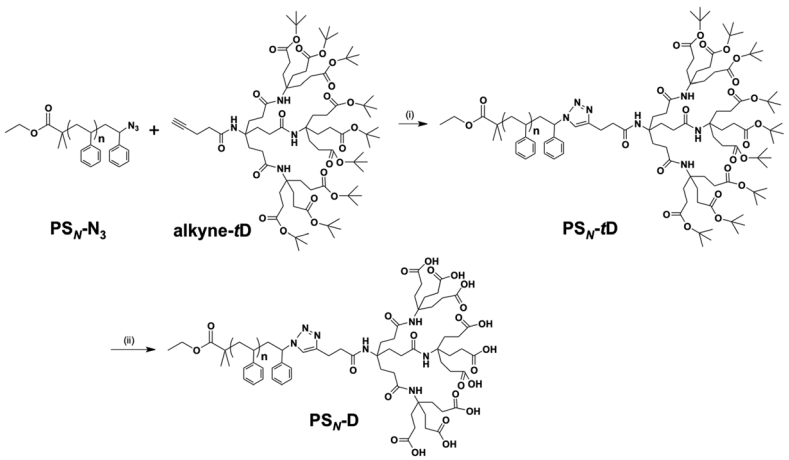

Scheme 1 General synthetic route of polystyrene–dendron giant conjugates (PS_N–D).[a] Reagents and conditions: (i) CuBr, PMDETA, alkyne–*t*D, toluene, r.t., 91%; (ii) trifluoroacetic acid, chloroform, r.t., 95%.

Table 1 Molecular characterizations of polystyrene–dendrons (PS_N–D) and their precursors

Label	M_n^{PS} [a] (g mol^{-1})	M_n^{total} [b] (g mol^{-1})	$Đ_M$ [c]	f_{PS} [d]	Phase structure[e]	d spacing[f] (nm)
PS_{16}–D	1600	2600	1.07	0.65	Lam	6.7
PS_{19}–D	1900	2900	1.03	0.69	Lam	7.3
PS_{24}–D	2400	3400	1.03	0.74	DG	7.1
PS_{28}–D	2800	3800	1.03	0.76	Hex	7.6
PS_{35}–D	3500	4500	1.04	0.80	Hex	7.9
PS_{60}–D	6000	7000	1.05	0.87	Hex	9.2
PS_{62}–D	6200	7200	1.07	0.88	Hex	9.3
PS_{67}–D	6700	7700	1.03	0.89	Hex	9.6
PS_{80}–D	8000	9000	1.04	0.90	Hex	10.2
PS_{82}–D	8200	9200	1.03	0.90	BCC	10.6
PS_{91}–D	9100	10 100	1.03	0.91	BCC	10.8
PD_{150}–D	15 000	16 000	1.04	0.95	Disorder	N/A

[a] Molecular weights measured by SEC calibrated with PS standards. [b] Molecular weights are calculated as a sum of PS_N and carboxylic acid functionalized dendron (D). [c] Molecular weight distributions of precursors measured by SEC. [d] Volume fractions of PS_N, calculated based on eqn (1). [e] Phase structures determined based on SAXS and TEM. [f] Domain sizes determined by primary peak on SAXS pattern.

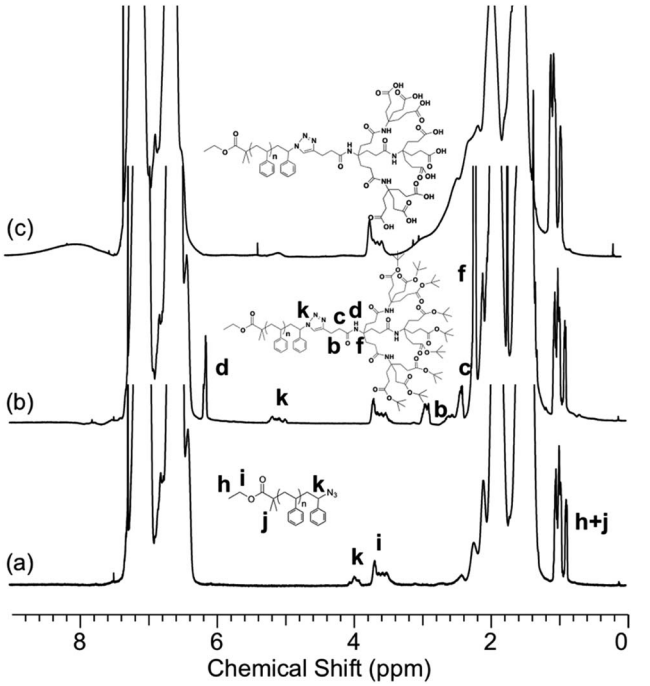

Fig. 1 ^{1}H NMR spectra of (a) PS_N–N_3; (b) PS_N–tD; and (c) PS_N–D. The results are based on the samples with $N = 19$.

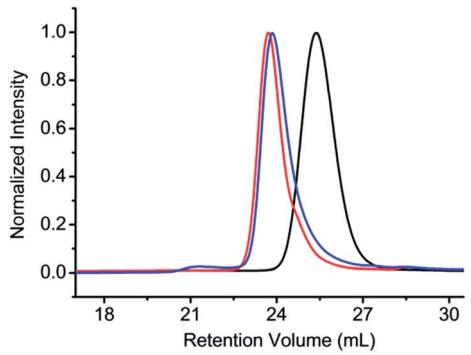

Fig. 2 SEC chromatograms of PS_N (black); PS_N–tD (red); and PS_N–D (blue). The results are based on the samples with $N = 19$.

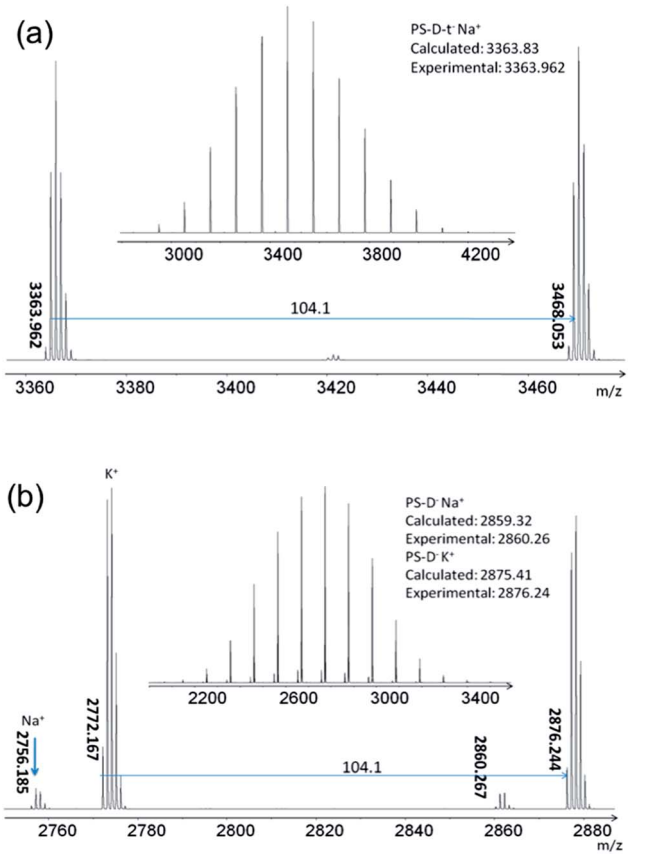

Fig. 3 MALDI-TOF mass spectra of PS_N–tD (a) and PS_N–D (b). The results were based on the samples with $N = 19$.

increases after the "click" reaction, as compared to its precursor (Fig. 2, black).

To further characterize the molecular structure, MALDI-TOF MS was utilized. Fig. 3a shows MALDI-TOF MS of PS_N–tD with $N = 19$. A mono-distribution with a molecular weight of 3363.96 is observed, which is in good accord with the calculated value (3363.83) confirming the structural assignment as well as the stability of the giant conjugates.

The *t*-butyl groups are completely removed, resulting in the formation of carboxylic acid functionalized dendron, as shown in Scheme 1. The resonance of the *t*-butyl groups disappeared in its NMR spectrum. Interestingly, the signals for dendron (b, c, d, and f) either disappear completely or can not be distinguished clearly, while those signals from PS_N tails are still observable (Fig. 1c). Correspondingly, the signals from dendron in ^{13}C NMR have also vanished, leaving only the PS_N signals (Fig. S4 in ESI†).

In Fig. 2, a shoulder is noted in SEC trace at low elution volume side (blue). These abnormal phenomena may be explained by rapid aggregation of the carboxylic acid functionalized dendrons in solution, as reported by others.[57–59] In MALDI-TOF MS, two distributions are observed, corresponding to the same molecule ionized with Na^+ and K^+, respectively (Fig. 3b). The accordance of molecular weight clearly provides unambiguous evidence of the structure of the final desired product, PS_N–D. The detailed molecular characterizations are listed in Table 1.

Self-assembly behaviour in the condensed state

By introducing the concept of giant polymer–dendron conjugates, in which the head unit keeps constant both in chemistry and size, while the length of tail varies, we then examined how the N, χ, and f_{PS} influence the phase structures. First, we investigated the effect of dendron's end groups on phase separation: the *t*-butyl groups *versus* the carboxylic acid groups (Scheme 1). Before the removal of the nine *t*-butyl end groups, this series of giant PS_N–tD conjugates do not exhibit any phase separation between the tD heads and PS_N tails (no ordered structures are formed) as evidenced in SAXS and TEM observations (Fig. S5a and b in ESI†), indicating that the χN must be smaller than the critical value required for the phase separation.[2] Removing the *t*-butyl groups leads to nine carboxylic acid groups on the periphery of the dendron head, which enhance the interaction

parameter χ between the dendron and PS_N by introducing collective hydrogen bonds. The effect drives the χN to exceed the critical value, and leads to phase separation.

Lamellar structures can be observed in the case of PS_{16}–D with an $f_{PS} = 0.65$ *via* SAXS experiments as shown in Fig. 4a. Two sharp scattering peaks can be clearly identified with a q-ratio of 1 : 2, indicating the existence of a long-range ordered Lam structure. The periodic spacing is calculated to be 6.7 nm based on the q value of the first order peak ($d = 2\pi/q$). The Lam structure has also been identified in the real space *via* TEM experiments as shown in Fig. 4b. The periodic dark and light grey layers are observed with an overall thickness of ~7 nm, agreeing well with the calculation based on SAXS results. The dark layers are the intensively stained dendron rich domains (*via* complex of carbonyl group and RuO_4)[60] and the light grey layers are shallowly stained PS_N tail rich domains. Their thicknesses are measured to be ~2.7 nm and ~4.3 nm, respectively.

By increasing the length of PS_N tail to $N = 24$, the PS_{24}–D conjugate's phase converts to a bicontinuous DG structure as confirmed by the SAXS and TEM observations. Fig. 4c shows a SAXS pattern of PS_{24}–D. Two scattering peaks with their q-value ratio of $\sqrt{6} : \sqrt{8}$, represents the typical profile of DG phase with $Ia\bar{3}d$ symmetry.[8,61] The domain spacing is calculated to be 7.1 nm, based on the q-value of the first-order peak. Fig. 4d is a bright field TEM image, which displays a wheel-like morphology, a typical projection of DG structure when observed from the [111] direction.[62] The distance between neighbouring wheel centers is ~7 nm, confirming the result obtained from the SAXS pattern. The interval of DG phase is rather narrow between the Lam and Hex phases compared with other morphological structures.

Fig. 4e shows a Hex structure that is identified based on the SAXS observation of PS_{53}–D with the $f_{PS} = 0.80$. The q-ratios of the observed three scattering peaks are $1 : \sqrt{3} : 2$, indicating the cylindrical packing. The structure is also confirmed by the TEM observation in the real space, within which both alternative layers and hexagonal packed patterns are observed when the viewing directions are along the [100] and [010], respectively. For this PS_{35}–D sample, the d-spacing calculated based on the SAXS is 7.6 nm (Fig. 4e), while 7.5 nm has been estimated from the TEM image (Fig. 4f).

Body-centred cubic-packed spheres can be found when the f_{PS} exceeds 0.90. Fig. 4g shows the scattering pattern of PS_{90}–D with an f_{PS} of 0.91. The q-ratio of the higher order peaks with first order is calculated to be $1 : \sqrt{2} : \sqrt{3} : 2$, indicating a BCC structure with a d-spacing of 10.8 nm. A square lattice pattern is also confirmed by the TEM bright field image that is a BCC structure viewed along the [001] (or [100]/[010]) direction as shown in Fig. 4h. The distance between neighbouring spheres is ~10 nm, agreeing well with the calculated value based on the SAXS result.

By further increasing the length of PS tail, the phase diagram enters the disorder state when the f_{PS} value approaches 1.0. No ordered structures could be identified, *e.g.*, in the case of PS_{150}–D in our SAXS and TEM experiments (Fig. S5c and d in ESI†). The detailed phase structure identifications of giant PS_N–D conjugates with varying length of PS tail are also included in Table 1.

In order to investigate the stability of these phase structures, temperature dependent SAXS experiments of these ordered structures are also conducted. Even at the temperatures reaching their decomposition temperatures (~180 °C), all of these ordered structures remain, indicating that these structures are stable in our experimental temperature range (see Fig. S6 in ESI†). This observation reveals that the effective χ parameter maintains above the critical value even at 180 °C.

Effects of molecular geometries on self-assembly

A phase diagram can thus be constructed according to the results obtained experimentally as shown in Fig. 5. Based on the SAXS and TEM results, four intervals of f_{PS} regions can be

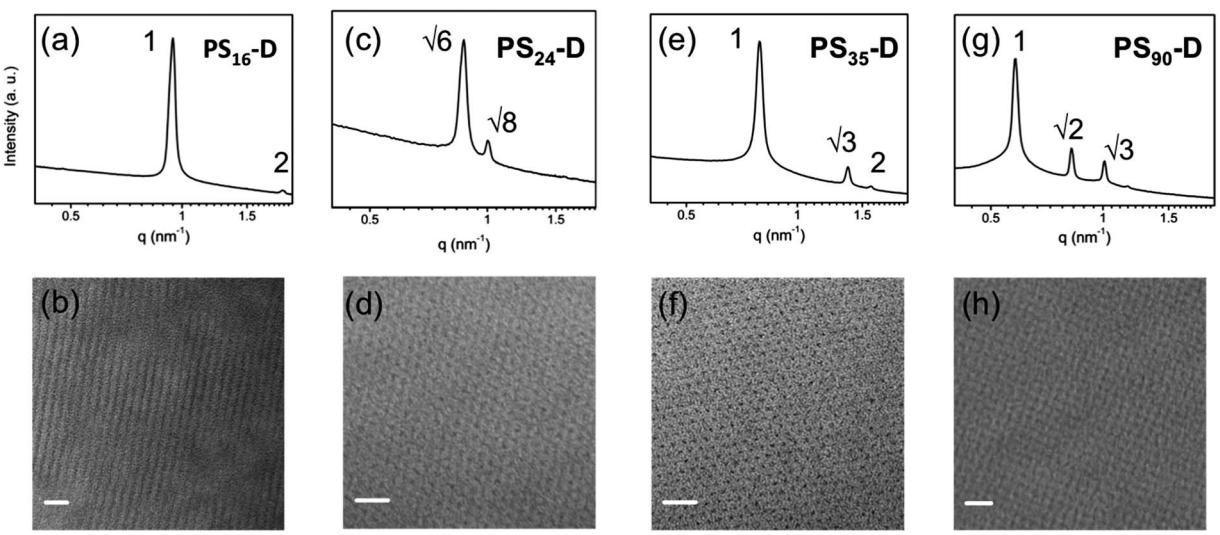

Fig. 4 SAXS patterns and TEM bright images for sample PS_{16}–D, Lam (a and b); PS_{24}–D, DG (c and d); PS_{30}–D, Hex (e and f); and PS_{90}–D, BCC (g and h).

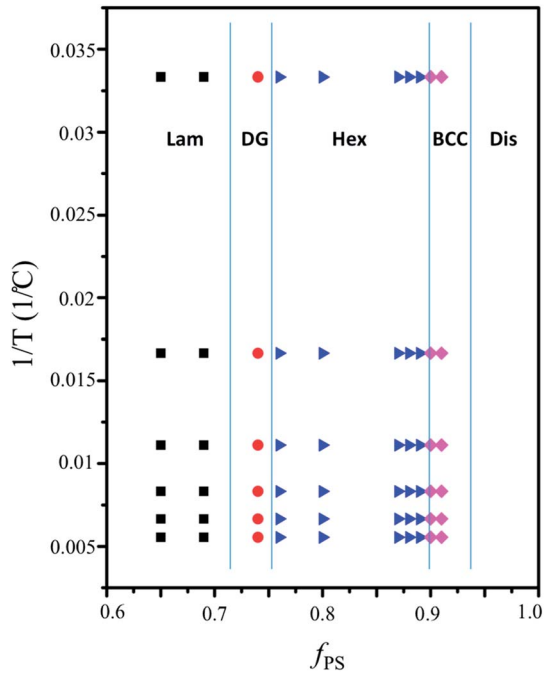

Fig. 5 Phase diagram of PS_N–D giant conjugates (Lam: lamellae; DG: bicontinues double gyriods; Hex: hexagonal packed cylinders; BCC: body-centered cubic packed spheres; and Dis: disorder).

estimated for the four structures (Lam: N/A–0.72; DG: 0.72–0.75; Hex: 0.75–0.90; and BCC: 0.90–0.94). Note that a precise phase boundary cannot be identified unless a continuous variation of PS_N tail length is available. In this phase diagram the phase boundaries are assumed to be at the middle of two neighboring phases based on samples studied by us.

The first observation in our experimentally determined phase diagram is that it is similar to the phase diagram of linear flexible diblock polymers. Specifically, four ordered phase structures having a sequence of Lam, DG, Hex, and BCC with increasing the f_{PS} was observed. However, we are not able to obtain phase information between $0 < f_{PS} < \sim 0.65$, due to the fact that decreasing the f_{PS} value can only be obtained by shortening the PS tail length since the size of dendron is fixed. For the samples in the $0 < f_{PS} < \sim 0.65$ region, the PS tails have to be extremely short, and they are very difficult to synthesize *via* a control/living radical polymerization with reasonably narrow polydispersity.

It is interesting to compare the phase diagram of the giant polymer–dendron conjugate with the corresponding linear diblock copolymers. Phase behaviours of a linear diblock copolymer system, polystyrene-*block*-poly(acrylic acid) (PS-*b*-PAA), that can be viewed as a linear analogue of this series of PS_N–D system, has been reported by Bendejacq *et al.*[63] A lamellar structure was observed in PS_{20}-*b*-PAA_{30} (its overall molecular weight is 4040 g mol^{-1}, $N = \sim 50$) with a f_{PS} of 0.51 and domain size of 16.4 nm. On the other hand, a Hex phase structure was observed in a PS_{45}-*b*-PAA_{170} (its overall molecular weight is 16 800 g mol^{-1}) with a f_{PS} of 0.27. If assuming symmetrical phase diagram in this linear polymer system, a Hex phase must also be observed when $f_{PS} = 0.73$.[7] However, in the PS_N–D system this composition results in a double gyroid phase (Fig. 5). No well-defined structure was observed when $f_{PS} = 0.88$ in a PS_{130}-*b*-PAA_{24} (its overall molecular weight is 14 700 g mol^{-1}). The comparison between the PS_N–D and its linear analogue PS-*b*-PAA indicates the boundary between neighboring phases of PS_N–D is shifted to higher f_{PS} values.[7,63] This leads to a somewhat asymmetrical shape of the phase diagram.[41,49,50] It can also be confirmed by comparing with the theoretically predicted phase diagram of conformationally symmetric diblock polymers.[7] Indeed, the region of Lam is found up to $f_{PS} = 0.7$ in the PS_N–D system while the calculated f in conformationally symmetric diblock copolymers is 0.62 as predicted by mean-field theory.[7] The boundary of Hex phase in the PS_N–D system appears between $f_{PS} = 0.75$ and 0.9, compared with the calculated f between 0.65 and 0.82 for linear flexible diblock polymers.[7] It should be noticed that the PS-*b*-PAA samples used by Bendejacq *et al.* are polydisperse with $Đ_M$ around 2.[63] It is well-established that polydispersity can lead to an increase of the domain spacing and decrease of the critical χN value.[64,65] On the other hand, the effect of polydispersity is not significant when compared with the large shift of the phase boundaries and domain spacing observed in the PS_N–D samples. The difference between the PS-*b*-PAA and PS_N–D must be induced by the curved interface between polymer domain and dendron domain as predicted theoretically.[40] The asymmetrical architecture at the interface forces the interfacial curvature toward the PS tails to alleviate the overcrowding of dendrons by providing significant interfacial area.[51] Since the phase structures are associated with interfacial curvature, it requires excess PS tails to balance the interfacial stretches to maintain a specific structure, and leads to shifts of the phase boundaries toward larger f_{PS} values.

However, a question may also arise: how does the change in density with temperature affect the f_{PS} changes in the phase diagram? This has to be associated with the temperature dependences of the PS and the dendron densities. Since the density of polymer is proportional to absolute temperature,[66,67] a linear relationship can be fitted using the density data of PS as reported in literatures[62] and measured density of dendron in this study, respectively, as shown in Fig. S7 and S8 in ESI.† Both densities of PS and dendron slightly decrease with increasing temperature, with a slop of 0.00036 and 0.00047. The temperature dependence of f_{PS} values can thus be calculated based on eqn (1) (summarized in Table S1 in ESI†). The f_{PS} values are found to be very slightly changed with varying temperature.

Generally speaking, ordered structures can be induced when the immiscibility (χN) between two blocks exceeds a critical value. For majority of linear flexible diblock copolymers, the χ value between two blocks is relatively small and thus, one requires a high N value to reach sufficient immiscibility. This requirement makes ordered structures with sub-10 nm size difficult to achieve in the linear flexible diblock polymers. For example, PS-*b*-PEO usually requires a minimum overall molecular weight of 16 kg mol^{-1} for the entire copolymer to enter strong phase segregation limit, corresponding to a domain size of 18–20 nm.[55,68] Although the χ between PS and PAA is much larger than normal flexible blocks (estimated to be ~0.0.3),[63,69] it

still requires an N value over fifty to reach weak segregation limit.[69] Even higher N is required to insure phase separation with sharp interface.

However, when taking geometrical effect into consideration, ordered structures could be prepared at relatively small N values with small domain sizes due to the ability of increasing the immiscibility. By incorporating a dendritic architectural component, a strong phase separation could be achieve with $N = 16$ (Fig. 4a) which is significantly lower than that of linear PS-*b*-PAA. Densely packed carboxylic acid functional groups on the surface of dendron facilitate the formation of collective hydrogen bonds, which are much stronger than the sum of corresponding mono-hydrogen bond.[70] Based on the fact that the PS_{16}–D forms well-ordered lamellae, it can be concluded that the χ value must be larger than the critical value at order–disorder transition ($\chi N = 10.5$). With an overall $N \sim 25$ for PS_{16}–D, a lower bound of χ value at $\sim$0.4 can be estimated. In the phase diagram, the transition boundary between ordered state and disordered state is then shifted vertically down (towards the high temperature) as compared to PS-*b*-PAA system.

The increase of the effective χ value by the increased attraction between the dendrons can be understood from the observation that, for an A–B binary mixture, the χ is an effective interaction parameter quantifying the mixing energy, $\chi = \frac{z}{k_B T}(2u_{AB} - u_{AA} - u_{BB})$, where u_{AB} are the nearest-neighbor interaction energy between A-monomer and B-monomer and z is the coordinate number of the lattice.[71] From this simple expression it is clear that the χ value can be increased by increasing the AB interaction energy, or decreasing the AA or BB interaction energy. The introduction of the hydrogen bonding sites to the dendron can be viewed as a large reduction in the dendron–dendron interaction energy and thus, a large increase of the effective χ value.

Conclusions

In summary, a series of giant PS_N–D conjugates was synthesized *via* a combination of "click" chemistry with controlled/living free radical polymerization. The self-assembly behaviour of the samples has been examined by SAXS and TEM experimental techniques. Four phases in linear flexible diblock copolymer systems are observed, including Lam, DG, Hex, and BCC structures. The dendritic geometry not only enhances the immiscibility that makes sub-10 nm phase separated domain sizes possible by modifying the geometric topologies of diblock copolymers, but also shifts the boundaries between neighbouring phases to larger f_{PS} values. The former may be induced by the collective hydrogen bonds among the carboxylic acid end groups at the dendron's periphery, and lead to an increase of the χ value; while the later may be attributed to curve interface induced by dendritic architecture. This study provides important insight towards the geometrical factor(s) that may influence the phase structure behaviours in addition to the considerations of χ, N, and f. This approach may be useful in tailored constructions of ordered patterns with sub-10 nm feature size.

Author contributions

The manuscript was written through contributions of all authors. All authors have given approval to the final version of the manuscript.

Conflict of interest

The authors declare no competing financial interest.

Acknowledgements

This work was supported by National Science Foundation (DMR-0906898). SZDC and WBZ acknowledge support from The Joint-Hope Education Foundation. ACS acknowledges the support by the Natural Science and Engineering Research Council (NSERC) of Canada. The synchrotron SAXS experiments were carried out at NSLS in BNL supported by DOE.

References

1 F. S. Bates and G. H. Fredrickson, *Annu. Rev. Phys. Chem.*, 1990, **41**, 525.
2 F. S. Bates, *Science*, 1991, **251**, 898.
3 E. Helfand, *Macromolecules*, 1975, **8**, 552.
4 E. Helfand and Z. R. Wasserman, *Macromolecules*, 1976, **9**, 879.
5 L. Leibler, *Macromolecules*, 1980, **13**, 1602.
6 S. T. Milner and P. D. Olmsted, *J. Phys. II*, 1997, **7**, 249.
7 M. W. Matsen and F. S. Bates, *Macromolecules*, 1996, **29**, 1091.
8 E. L. Thomas, D. B. Alward, D. J. Kinning, D. C. Martin, L. Dale, J. Handlin and L. J. Fetters, *Macromolecules*, 1986, **19**, 2197.
9 K. Almdal, K. A. Koppi, F. S. Bates and K. Mortensen, *Macromolecules*, 1992, **25**, 1743.
10 I. W. Hamley, K. A. Koppi, J. H. Rosedale and F. S. Bates, *Macromolecules*, 1993, **26**, 5959.
11 D. A. Hajduk, P. E. Harper, S. M. Gruner, C. C. Honeker, G. Kim, L. E. Thomas and L. J. Fetters, *Macromolecules*, 1994, **27**, 4603.
12 M. Schulz, F. Bates, K. Almdal and K. Mortensen, *Phys. Rev. Lett.*, 1994, **73**, 86.
13 L. Zhu, P. Huang, S. Z. D. Cheng, Q. Ge, R. Quirk, E. Thomas, B. Lotz, J.-C. Wittmann, B. Hsiao, F. Yeh and L. Liu, *Phys. Rev. Lett.*, 2001, **86**, 6030.
14 R.-M. Ho, Y.-W. Chiang, C.-C. Tsai, C.-C. Lin, B.-T. Ko and B.-H. Huang, *J. Am. Chem. Soc.*, 2004, **126**, 2704.
15 K. K. Tenneti, X. Chen, C. Y. Li, Y. Tu, X. Wan, Q.-F. Zhou, I. Sics and B. S. Hsiao, *J. Am. Chem. Soc.*, 2005, **127**, 15481.
16 N. Hadjichristidis, *J. Polym. Sci., Part A: Polym. Chem.*, 1999, **37**, 857.
17 L.-P. Yang, X.-H. Dong and C.-Y. Pan, *J. Polym. Sci., Part A: Polym. Chem.*, 2008, **46**, 7757.
18 H. Gao, *Macromol. Rapid Commun.*, 2012, **33**, 722.
19 B. A. Laurent and S. M. Grayson, *J. Am. Chem. Soc.*, 2006, **128**, 4238.

20 B. A. Laurent and S. M. Grayson, *Chem. Soc. Rev.*, 2009, **38**, 2202.
21 R. L. Lescanec, D. A. Hajduk, G. Y. Kim, Y. Gan, R. Yin, S. M. Gruner, T. E. Hogen-Esch and E. L. Thomas, *Macromolecules*, 1995, **28**, 3485.
22 J. E. Poelma, K. Ono, D. Miyajima, T. Aida, K. Satoh and C. J. Hawker, *ACS Nano*, 2012, **12**, 10845.
23 J. N. Hoskins and S. M. Grayson, *Polym. Chem.*, 2011, **2**, 289.
24 D. Yan, Y. Zhou and J. Hou, *Science*, 2004, **303**, 65.
25 C. Gao and D. Yan, *Prog. Polym. Sci.*, 2004, **29**, 183.
26 F. Wurm and H. Frey, *Prog. Polym. Sci.*, 2011, **36**, 1.
27 K. Matyjaszewski, *Macromolecules*, 2012, **45**, 4015.
28 D. J. Keddie, G. Moad, E. Rizzardo and S. H. Thang, *Macromolecules*, 2012, **45**, 5321.
29 M. Park, *Science*, 1997, **276**, 1401.
30 D. J. C. Herr, *J. Mater. Res.*, 2011, **26**, 122.
31 J. D. Cushen, C. M. Bates, E. L. Rausch, L. M. Dean, S. X. Zhou, C. G. Willson and C. J. Ellison, *Macromolecules*, 2012, **45**, 8722.
32 X. Yu, K. Yue, I. F. Hsieh, Y. Li, X. H. Dong, C. Liu, Y. Xin, H. F. Wang, A. C. Shi, G. R. Newkome, R. M. Ho, E. Q. Chen, W. B. Zhang and S. Z. Cheng, *Proc. Natl. Acad. Sci. U. S. A.*, 2013, **110**, 10078.
33 K. Kempe, K. L. Killops, J. E. Poelma, H. Jung, J. Bang, R. Hoogenboom, H. Tran, C. J. Hawker, U. S. Schubert and L. M. Campos, *ACS Macro Lett.*, 2013, 677.
34 J. He, J. Y. Wang, J. Xu, R. Tangirala, D. Shin, T. P. Russell, X. Li and J. Wang, *Adv. Mater.*, 2007, **19**, 4370.
35 J. Xu, S. W. Hong, W. Gu, K. Y. Lee, D. S. Kuo, S. Xiao and T. P. Russell, *Adv. Mater.*, 2011, **23**, 5755.
36 I. Nakamura, N. P. Balsara and Z.-G. Wang, *Phys. Rev. Lett.*, 2011, **107**, 198301.
37 S. H. Kim, M. J. Misner, L. Yang, O. Gang, B. M. Ocko and T. P. Russell, *Macromolecules*, 2006, **39**, 8473.
38 W.-S. Young and T. H. Epps, *Macromolecules*, 2009, **42**, 2672.
39 C. M. Bates, T. Seshimo, M. J. Maher, W. J. Durand, J. D. Cushen, L. M. Dean, G. Blachut, C. J. Ellison and C. G. Willson, *Science*, 2012, **338**, 775.
40 S. T. Milner, *Macromolecules*, 1994, **27**, 2333.
41 A. Frischknecht and G. H. Fredrickson, *Macromolecules*, 1999, **32**, 6831.
42 A. N. Morozov and J. G. E. M. Fraaije, *J. Chem. Phys.*, 2001, **114**, 2452.
43 G. Grason, B. DiDonna and R. Kamien, *Phys. Rev. Lett.*, 2003, **91**, 058304.
44 M. W. Matsen and F. S. Bates, *J. Polym. Sci., Part B Polym. Phys.*, 1996, **35**, 945.
45 J. R. Bell, K. Chang, C. R. López-Barrón, C. W. Macosko and D. C. Morse, *Macromolecules*, 2010, **43**, 5024.
46 B. M. Rosen, C. J. Wilson, D. A. Wilson, M. P. R. Imam and V. Percec, *Chem. Rev.*, 2009, **109**, 6275.
47 J. M. J. Fréchet and D. A. Tomalia, *Dendrimer and Other Dendritic Polymers*, John Wiley & Sons, West Sussex, 2001.
48 G. R. Newkome, C. N. Moorefield and F. Vögtle, *Dendrimers and Dendrons: Concepts, Syntheses, Applications*, Wiley-VCH, Weinheim, Germany, 2004.
49 C. Roman, H. R. Fischer and E. W. Meijer, *Macromolecules*, 1999, **32**, 5525.
50 M. E. Mackay, Y. Hong, M. Jeong, B. M. Tande, N. J. Wagner, S. Hong, S. P. Gido, R. Vestberg and C. J. Hawker, *Macromolecules*, 2002, **35**, 8391.
51 D. J. Pochan, L. Pakstis, E. Huang, C. Hawker, R. Vestberg and J. Pople, *Macromolecules*, 2002, **35**, 9239.
52 M. A. Johnson, J. Iyer and P. T. Hammond, *Macromolecules*, 2004, **37**, 2490.
53 G. R. Newkome, R. K. Behera, C. N. Moorefield and G. R. Baker, *J. Org. Chem.*, 1991, **56**, 7162.
54 W.-B. Zhang, Y. Tu, R. Ranjan, R. M. V. Horn, S. Leng, J. Wang, M. J. Polce, C. Wesdemiotis, R. P. Quirk, G. R. Newkome and S. Z. D. Cheng, *Macromolecules*, 2008, **41**, 515.
55 L. Zhu, Y. Chen, A. Zhang, B. H. Calhoun, M. Chun, R. P. Quirk and S. Z. D. Cheng, *Phys. Rev. B: Condens. Matter Mater. Phys.*, 1999, **60**, 10022.
56 X.-H. Dong, W.-B. Zhang, Y. Li, M. Huang, S. Zhang, R. P. Quirk and S. Z. D. Cheng, *Polym. Chem.*, 2012, **3**, 124.
57 J. C. M. v. Hest, M. W. P. L. Baars, C. Elissen-Romhn, M. H. P. v. Genderen and E. W. Meijer, *Macromolecules*, 1995, **28**, 6689.
58 J. C. M. v. Hest, D. A. P. Delnoye, M. W. P. L. Baars, M. H. P. v. Genderen and E. W. Meijer, *Science*, 1995, **268**, 1592.
59 J. C. M. v. Hest, D. A. P. Delnoye, M. W. P. L. Baars, M. H. P. v. Genderen and E. W. Meijer, *Chem.–Eur. J.*, 1996, **2**, 1616.
60 J. S. Trent, J. I. Scheinbeim and P. R. Couchman, *Macromolecules*, 1983, **16**, 589.
61 I. W. Hamley and V. Castelletto, *Prog. Polym. Sci.*, 2004, **29**, 909.
62 I. Vukovic, T. P. Voortman, D. H. Merino, G. Portale, P. Hiekkataipale, J. Ruokolainen, G. ten Brinke and K. Loos, *Macromolecules*, 2012, **45**, 3503.
63 D. Bendejacq, V. Ponsinet, M. Joanicot, Y. L. Loo and R. A. Register, *Macromolecules*, 2002, **35**, 6645.
64 D. M. Cooke and A.-C. Shi, *Macromolecules*, 2006, **39**, 6661.
65 N. A. Lynd, A. J. Meuler and M. A. Hillmyer, *Prog. Polym. Sci.*, 2008, **33**, 875.
66 A. Bondi, *J. Phys. Chem.*, 1964, **68**, 441.
67 J. C. McGowan, *Polymer*, 1969, **10**, 841.
68 L. Zhu, S. Z. D. Cheng, B. H. Calhoun, Q. Ge, R. P. Quirk, E. L. Thomas, B. S. Hsiao, F. Yeh and B. Lotz, *Polymer*, 2001, **42**, 5829.
69 J. Cheng, R. A. Lawson, W.-M. Yeh, N. D. Jarnagin, A. Peters, L. M. Tolbert and C. L. Henderson, in *Conference on Alternative Lithographic Technologies IV*, ed. W. M. Tong and D. J. Resnick, San Jose, CA, 2012, vol. 8323.
70 M. Mammen, S.-K. Choi and G. M. Whitesides, *Angew. Chem., Int. Ed.*, 1998, **37**, 2754.
71 M. Rubinstein and R. H. Colby, *Polymer Physics*, Oxford University Press, Oxford, 2003.

